Study of Some He^3-Induced Reactions on C^{12}

D. A. Bromley, E. Almqvist, H. E. Gove, A. E. Litherland, E. B. Paul,* and A. J. Ferguson
Chalk River Laboratory, Atomic Energy of Canada Limited, Chalk River, Ontario, Canada
(Received October 29, 1956)

He^3-induced reactions in carbon have been studied for bombarding energies in the range 1.0 to 3.0 Mev. Absolute excitation curves have been obtained for the proton groups leading to the first three states in N^{14} and for the neutron group leading to the O^{14} ground state; these show pronounced resonance structure corresponding to levels in O^{15}. Angular distributions have been measured at seven different energies for protons and four for neutrons. These distributions are not directly explicable as resulting from either compound nucleus or direct interaction processes but do show marked structure. The threshold for the $C^{12}(He^3,n)O^{14}$ reaction has been determined to be 1449.6±2.8 kev, which requires a mass defect for O^{14} of 12.146±0.0065 Mev. The total cross sections for the (He^3,n) reaction to the O^{14} ground state and for the (He^3,p) reaction to the analog 2.3-Mev state in N^{14} are in the ratio 2:1, and the angular distributions for protons and neutrons from these reactions are quite similar at energies somewhat above the neutron threshold, as would be expected. The total cross sections for the (He^3,p) reaction range from 0.03 to 25 mb at these energies. The cross section of the $C^{12}(He^3,\alpha_0)C^{11}$ reaction has been found to be approximately an order of magnitude greater than that of the $C^{12}(He^3,n_0)O^{14}$ reaction and is suggestive of direct interaction.

INTRODUCTION

THE He^3 beam from the Chalk River electrostatic generator has been used in a study of some He^3-induced reactions on carbon. Such a study is particularly attractive since the characteristics of the final states were relatively well known, and it was hoped that measurements of the yields as well as energy and angular dependence of the cross sections of these reactions would provide the data for their detailed theoretical study; it was, furthermore, essential since a knowledge of these reaction characteristics is required in any program of study of He^3 reactions in correcting for the ubiquitous carbon contaminant on all targets.

The present paper will present the results of the study of the $C^{12}(He^3,p)N^{14}$ and the $C^{12}(He^3,n_0)O^{14}$ reactions and of a preliminary measurement of the $C^{12}(He^3,\alpha_0)C^{11}$ cross section. Some results of the $C^{12}(He^3,p\gamma)N^{14}$ work have previously been reported,[1] and these measurements have been extended. The $C^{12}(He^3,n_0)O^{14}$ reaction was of particular interest since it provides a new experimental check on the mass of O^{14}. Furthermore, since the O^{14} ground state and the 2.3-Mev level in N^{14} are members of an isobaric triplet, it was of interest to compare the angular distributions and relative yields of the neutrons and protons to these states from the same states in the compound nucleus O^{15}. Away from the neutron threshold the relative yields would be expected to be a function only of the isobaric spins involved in the two reactions.

The $C^{12}(He^3,p)N^{14}$ angular distribution has been measured previously at 2.0 Mev [2] and 4.5 Mev,[3] and also the threshold energy for the $C^{12}(He^3,n)O^{14}$ reaction.[4]

EQUIPMENT

Proton Detector

The experimental apparatus, used in the determination of the excitation curves as well as of the relative and total cross sections, is shown in Fig. 1. The He^3 beam of the accelerator passes through a hole in a liquid nitrogen trap before reaching the target to reduce contaminant build-up. The targets themselves are mounted on an insulated plate so that the total beam intercepted by the target can be measured and integrated in a manner to be described. As shown in the figure, the protons are detected by a CsI crystal coupled to an RCA 6655 photomultiplier, and the counter aperture is defined by tantalum apertures mounted over the crystal. A 0.0004-inch aluminum foil is stretched completely over the crystal, and a lead hood is then mounted to cover both the tantalum aperture and the end of the photomultiplier to provide some shielding from low-energy gamma radiation, to which the CsI crystals

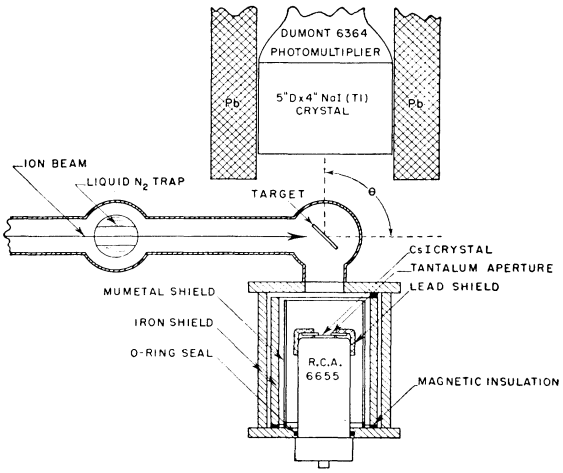

FIG. 1. Schematic view of the detection apparatus used for proton and proton-gamma experiments.

* Now at Atomic Energy Research Establishment, Harwell, England.

[1] Gove, Litherland, Almqvist, and Bromley, Phys. Rev. **103**, 835 (1956).

[2] R. Johnston and H. D. Holmgren, Bull. Am. Phys. Soc. Ser. II, **1**, 21 (1956).

[3] Johnston, Wolicki, Geer, and Holmgren, Bull. Am. Phys. Soc. Ser. II, **1**, 197 (1956).

[4] J. W. Butler, Bull. Am. Phys. Soc. Ser. II, **1**, 94 (1956).

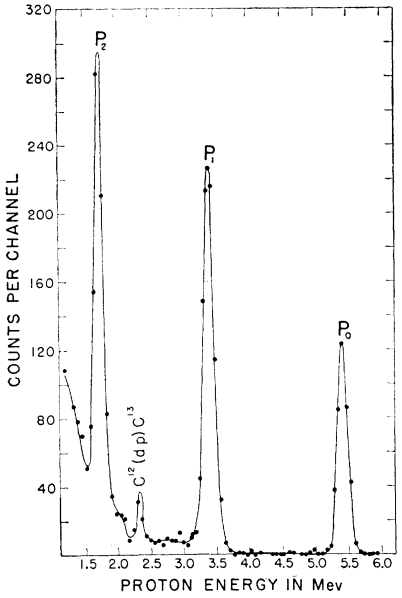

FIG. 2. Proton spectrum from $C^{12}(He^3,p)N^{14}$ at a bombarding energy of 1.3 Mev. The three major proton groups correspond to the formation of N^{14} in its ground and first two excited states. The weak group at about 2.3 Mev results from the ground state $C^{12}(d,p)C^{13}$ reaction. The deuterons involved have an energy of about 870 kev and result from the HD^+ component of the mass-3 beam. 43% He^3 gas was used in the ion source for this run; when 100% He^3 is used, this peak disappears.

are quite sensitive. Three coaxial magnetic shields are provided around the tube as shown, two of iron and one of mu metal. By inserting appropriate shims between the base of this structure and the tube base, the acceptance solid angle of the counter can be varied by a determined amount. We have used the counter with solid angles of 8.4×10^{-3} steradian and 4.6×10^{-3} steradian; as shown, it is fixed rigidly at 90° to the beam axis. A typical spectrum of protons from the $C^{12}(He^3,p)N^{14}$ reaction is shown in Fig. 2 where the instrumental resolution is approximately 3.5%, and the peaks are clearly resolved. From the kinematics of the reaction the small peak at about 2.3 Mev has been assigned to the ground state $C^{12}(d,p)C^{13}$ reaction. In measurements of total and relative cross section, apertures one-eighth inch in diameter were inserted into the beam tube immediately before the target to define more closely the beam extent and location, and a grid has also been used between this aperture and the target maintained at some 300 volts negative with respect to the target to suppress secondary electron emission. The beam current integrator uses conventional analog computer integrating circuits.[5]

Gamma Detector

Gamma radiation has been detected by using a five-inch diameter by four-inch deep NaI crystal; the technique has previously been described.[6] This crystal was mounted as shown (Fig. 1) and was free to rotate about a vertical axis centered on the target. This feature was of course necessary in determining the angular correlations of some of the gamma radiations observed in the $p\gamma$ coincidence work. In addition, to allow checking on the azimuthal variation of correlations, the proton counter was arranged so that it could be rotated through 90° out of the plane of the figure, leaving the gamma counter fixed. The outputs of these detectors, after shaping and amplification in conventional circuitry, were displayed either on a 30- or on an 80-channel analyzer. The circuitry used was such that the output of either counter in coincidence with any given section of the output spectrum of the other could be readily displayed on either or both kicksorters. In addition, the coincidence gate, through which either detector spectrum passes to the multichannel analyzers, could be opened by any selected part of these spectra. This "self-coincidence" arrangement allowed observation of exactly that part of the spectrum which was opening the gate, as is illustrated in a later figure (Fig. 21).

In determining the angular distributions of the protons from the $C^{12}(He^3,p)N^{14}$ reaction, we have used an angular distribution chamber which has been described elsewhere.[7] Briefly, the He^3 beam from the accelerator, after passing through a one-eighth inch diameter tantalum aperture, was incident on a thin target foil in the scattering chamber. The chamber allows continuous rotation of the detector in the angular range −145° to 0 to +145° in the laboratory system. A somewhat different detector geometry has been used with this chamber in that a CsI crystal cemented to the front face of a Dumont 6292 photomultiplier was covered with a conical surface coated with MgO for diffused reflection. A tantalum diaphragm at the entrance to this reflector cone resulted in an angular acceptance width of 2.3° and a detection solid angle of 5×10^{-3} steradian. A second, similar CsI

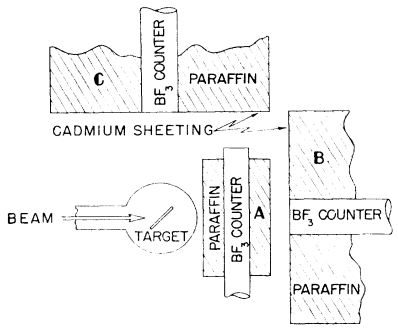

FIG. 3. Schematic view of the detection apparatus used for neutron experiments. The paraffin moderator on counter A is of rectangular cross section; those on counters B and C are cylindrical.

[5] W. A. Higinbotham and S. Rankowitz, Rev. Sci. Instr. **22**, 688 (1951).

[6] H. E. Gove and E. B. Paul, Phys. Rev. **97**, 104 (1955).

[7] R. L. Clarke and E. B. Paul (to be published).

crystal was used as a monitor in determining the angular distributions and was mounted at a fixed angle of 17° to the beam axis. Here again the output of the CsI detector was displayed on a 30- or 80-channel pulse height analyzer; the monitor output was connected to a single-channel analyzer in order that a voltage gate could be set to include only one or more of the proton groups in the reaction. All angular distribution data presented here are normalized to a given monitor count to compensate for possible changes in the target composition during the bombardment.

Neutron Detectors

The experimental equipment used in studying the neutron yield and angular distributions from the $C^{12}(He^3,n)O^{14}$ reaction is shown schematically in Fig. 3. The neutron counters contained BF_3 enriched to 99 atomic percent B^{10}.[8] The long counters, B and C, had cylindrical paraffin moderators 10.5 in. in diameter and 10.0 in. long, coaxial with a counter 1.5 in. in diameter and 9 in. long, with 0.020-in. cadmium sheeting over the units. The sensitivity of the long counters had been much improved by drilling a series of six evenly spaced holes 1.5 in. in diameter with their axes parallel to the counter axis in the annular paraffin moderator.[9,10] These detectors had a measured efficiency of 0.45% for 1-Mev neutrons. Figure 4 is a typical pulse height spectrum obtained by exposing one of the long counters to a Ra-Be neutron source mounted on the counter axis. The counter resolution is seen to be adequate to separate pulses due to alpha transitions to the ground and first excited states of Li^7, and, in agreement with previous results,[11] the decay is of course predominantly to the first excited state. Integral biases have been set below the major peak and all counts greater than this bias have been taken as a measure of the neutron flux.

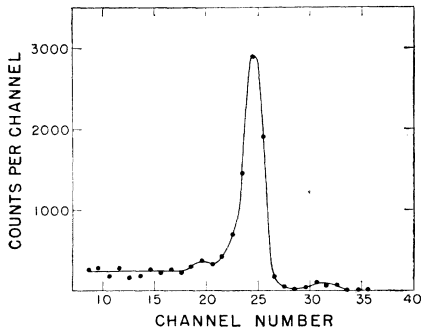

FIG. 4. Pulse spectrum from enriched BF_3 counter exposed axially to a Ra-Be neutron source. The weak high energy group corresponds to alpha transitions to the Li^7 ground state and the intense group to those to the Li^7 first excited state.

The threshold neutron counter consisted of a BF_3 counter 1-in. in diameter and 3-in. long in a 2.5×2.5×4.0-in. block of paraffin. The efficiency of this detector was measured to be about 0.30% for neutron energies between 0.3 and 0.8 Mev. With the arrangement shown in Fig. 3, the 0° and 90° excitation curves were obtained simultaneously with the ratio of the threshold counter to the 0° long-counter counting rates, which was used to fix the reaction threshold more reliably than was possible from observation of the excitation curves alone.[10]

In obtaining the neutron angular distributions, one of the long counters was mounted on a rotatable mount centered on the target; the threshold neutron counter previously described was mounted close to the target and was used as a monitor. The angular acceptance of this system was approximately ±10°.

Target Preparation

The targets used in this work were prepared by maintaining an arc discharge *in vacuo* between two high-purity graphite electrodes and supporting the target backings above the discharge. This provides a simple and convenient method of preparing carbon targets of high purity, over a wide range of thicknesses, on a variety of backings. For the angular distribution measurements we have used backings of 0.0004-in. aluminum. This thickness was chosen as being adequate to stop the He^3 ions from entering and jamming the photodetectors at forward angles while still having a negligible effect on the protons, as well as to prevent the occurrence of (He^3,p) reactions on the carbon deposits on slit edges and counter surfaces. For some of the gamma work 0.020-in. tantalum backings were used. The thickness of the carbon targets has been determined by using aluminum backings and examining the yield of 11-Mev gamma radiation from the $Al^{27}(p,\gamma)Si^{28}$ reaction in the vicinity of the 993.3-kev resonance,[12] first with the target reversed and the proton beam striking the exposed target backing and secondly with the target in the normal position and the beam traversing the carbon deposit before striking the aluminum. Figure 5 shows the excitation curves obtained in this energy region; from the observed energy shift of the step in the gamma radiation yield, the target thickness is found for 993-kev protons and is then converted into thickness in $\mu g/cm^2$ using the energy loss data as given by Aron.[13] The targets used were in the range from 20 to 100 $\mu g/cm^2$.

Energy Calibration

The energy of the He^3 beam incident on the target in these experiments was determined in the usual way by

[8] We are indebted to Mr. I. L. Fowler for supplying these BF_3 counters.

[9] A. O. Hansen and J. L. McKibben, Phys. Rev. **72**, 673 (1947).

[10] T. W. Bonner and C. F. Cook, Phys. Rev. **96**, 122 (1954).

[11] F. Ajzenberg and T. Lauritsen, Revs. Modern Phys. **27**, 77 (1955).

[12] Herb, Snowdon, and Sala, Phys. Rev. **75**, 246 (1949).

[13] W. A. Aron, University of California Radiation Laboratory Report UCRL-1325, May, 1951 (unpublished).

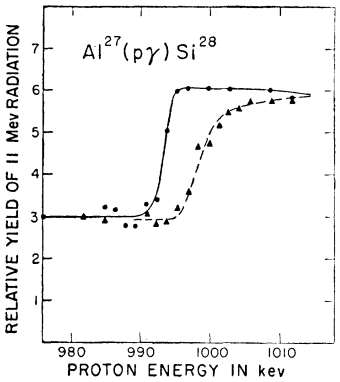

FIG. 5. Gamma-radiation yield in the vicinity of the 993-kev resonance in the $Al^{27}(p,\gamma)Si^{28}$ reaction. The closed circles were obtained with the proton beam striking the aluminum surface and the triangles when the beam first traversed the carbon deposit.

noting the frequency of the proton gyromagnetic resonance in the uniform magnetic field of the deflecting and energy-defining magnet. Two separate measurements are required to calibrate this particular technique. First, the absolute scale must be determined by comparison with accurately known threshold energies and resonance energies. Secondly, the linearity of this system must be investigated. Two separate determinations of the absolute calibration have been made using an elemental lithium target and the equipment previously described. Using the neutron detection apparatus, we have determined the frequency corresponding to the $Li^7(p,n)Be^7$ threshold which is given by Mattauch *et al.*[14] to be at 1881.6±0.45 kev. Secondly, and using the same lithium target, we have examined the yield of 9.28- and 4.82-Mev gamma radiation from the $Li^7(\alpha,\gamma)B^{11}$ reaction in the vicinity of the 958-kev resonance. The energy of this resonance has been given by Bennett, Roys, and Toppel[15] as 958±1 kev in terms of the $F^{19}(p,\alpha\gamma)O^{16}$ resonance at 873.5 kev. The energy scales for different particles in the beam were related by noting that the frequency at resonance is proportional to the momentum equal to $[2m_0T(1+T/2m_0c^2)]^{\frac{1}{2}}$. It should be noted that it is essential that accurate nuclear masses be used for the light particles involved, since otherwise errors of the order of tens of kilovolts are possible. The relativistic correction term (in parentheses) amounts to about 0.1% for the energies concerned here. Having established the energy scale with the $Li^7(p,n)Be^7$ reaction, the computed energy corresponding to the midpoint of the rise observed in the $Li^7(\alpha,\gamma)B^{11}$ gamma-radiation yield for both the 9.28- and 4.82-Mev radiation is 957.2±2 kev, which is in excellent agreement with the previously quoted value. Figure 6 shows a typical yield step obtained for these gamma radiations.

As a check on the linearity of the deflection system, we have examined the yield of 3.86- and 3.68-Mev gamma radiation from the $B^{10}(\alpha,p\gamma)C^{13}$ reaction in the vicinity of the 1.51-Mev resonance. Again taking the midpoint of the step in the thick target yield, we find an energy of 1.518±0.004 Mev, whereas the quoted value for this resonance is 1.51±0.010 Mev.[16] We have also examined the $Al^{27}(p,\gamma)Si^{28}$ reaction in the vicinity of the 993-kev resonance and find that the resonance energy is 995.7±3 kev, which is consistent with the quoted value of 993.3±1 kev.[12] The energy calibration was of particular importance in the measurement of the $C^{12}(He^3,n)O^{14}$ threshold. The calibration energies listed, which correspond to He^3 energies of 628 kev, 1271 kev, 2004 kev, and 332 kev, respectively, bracket the threshold energy which is at about 1450 kev.

RESULTS

Excitation Curves—$C^{12}(He^3,p)N^{14}$

Figure 2 is a typical pulse height spectrum of the protons from the $C^{12}(He^3,p)N^{14}$ reaction obtained at a bombarding energy of 1.30 Mev. Figure 7 shows spectra in the region corresponding to particles of energy greater than those from the $C^{12}(He^3,p)N^{14}$ reaction. Proton groups in this region are due to the indicated reactions, $He^3(d,p)He^4$, $He^3(He^3,p)Li^5$, on He^3 adsorbed on the target, and $C^{13}(He^3,p)N^{15}$ from the C^{13} present in the natural carbon targets. The deuterons are present in the HD^+ component of the mass-three beam. The strong resonance for the first of these reactions at $E_d\cong 430$ kev[11] causes the marked increase in yield in Part *A* of this figure. The total contribution from all these reactions is quite small and has been subtracted from the data presented. Figure 8 is the excitation curve for the proton groups leading to the formation of N^{14} in its ground and first two excited states, all measured at 90° to the incident beam. The low-energy sections of these excitation curves have been plotted on an expanded scale for clarity. Since the angular distributions change quite rapidly with energy, particularly in the region of the higher resonances, a measurement of the total cross section as a function of energy would be required to locate accurately the resonances and corresponding levels in O^{15}. The resonance energies to be quoted herein

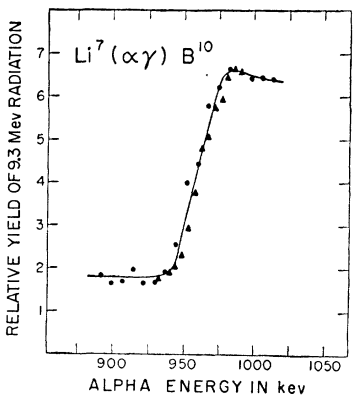

FIG. 6. Gamma-radiation yield in the vicinity of the 958-kev resonance in the $Li^7(\alpha,\gamma)B^{11}$ reaction. Similar curves were also measured for the 4.8-Mev radiation yield. The circular and triangular points were obtained using different lithium targets.

[14] Mattauch, Waldmann, Bieri, and Everling, Z. Naturforsch. **11**, 525 (1956).
[15] Bennett, Roys, and Toppel, Phys. Rev. **82**, 20 (1951).
[16] Shire, Wormald, Lindsay-Jones, Lundén, and Stanley, Phil. Mag. **44**, 1197 (1953).

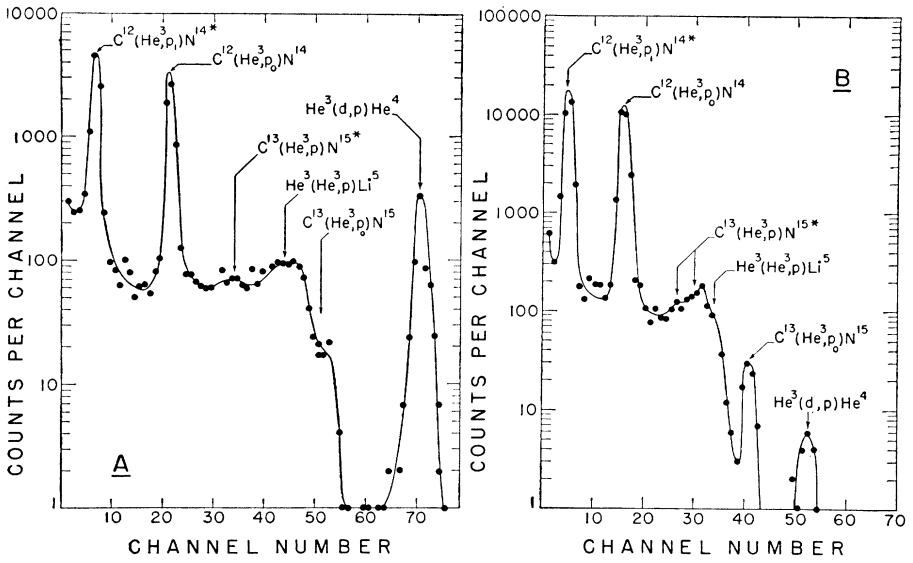

FIG. 7. These curves show proton spectra in the energy interval above the groups from $C^{12}(He^3,p)N^{14}$ and give a measure of the amount of background present. Curves *A* and *B* were obtained for bombarding He^3 energies of 1.3 and 2.4 Mev, respectively.

refer therefore to the approximate energies at which the 90° excitation curves peak. The slight apparent shift of the peak positions in these curves toward higher energies with increasing proton energy could be explained on this basis. Measurements have been made at intervals of approximately 22.5 kev over the entire curves and at closer intervals in the region of the low resonances. The absolute cross sections indicated on the ordinate scale in this figure were measured as described in the following section.

The weak resonance at 1.21 Mev feeding the ground and second excited state of N^{14} corresponds to a state in O^{15} at 13.10±0.02 Mev in agreement with that observed at 13.09 Mev in the $N^{14}(p,\alpha)C^{11}$ reaction.[17] The resonances at 1.3, 2.15, 2.5, and 2.7 Mev, and the strong resonance which is beginning to appear in these yield curves slightly above 2.9 Mev, correspond to previously unobserved states in O^{15} at about 13.2, 13.8, 14.1, 14.3, and 14.4 Mev, respectively. Although the proton group to the 4.9-Mev third excited state of N^{14}

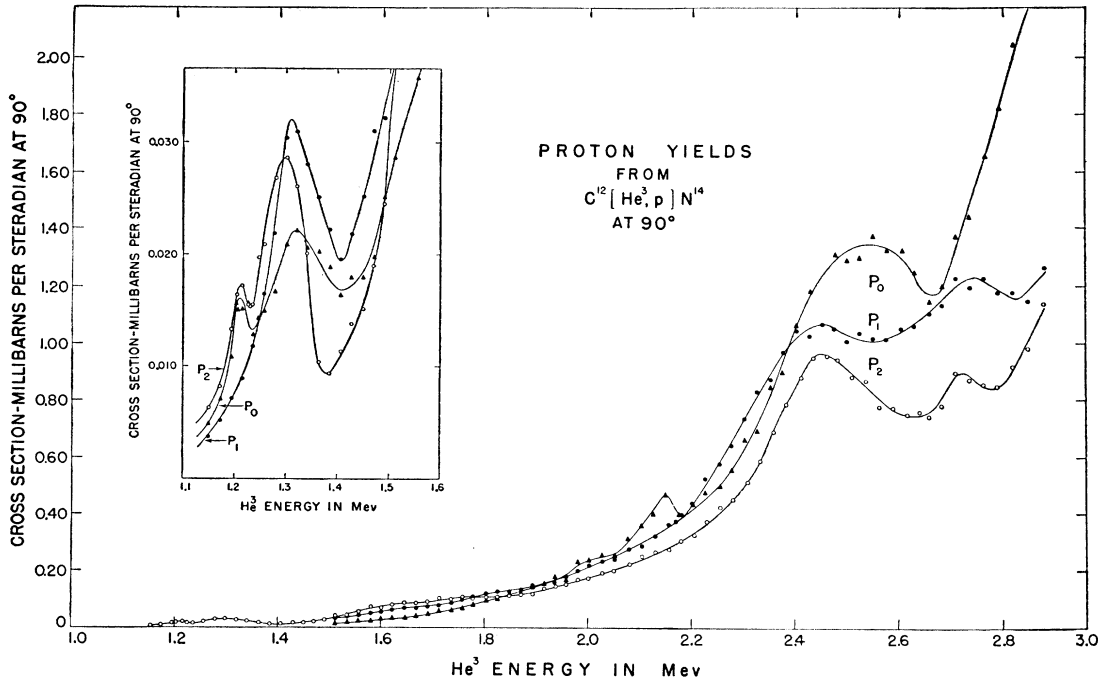

FIG. 8. Excitation curves for protons from $C^{12}(He^3,p)N^{14}$ corresponding to formation of N^{14} in its ground and first two excited states. The low-energy region has been replotted in the inset figure with an expanded ordinate.

[17] Blaser, Marmier, and Sempert, Helv. Phys. Acta **25**, 442 (1952).

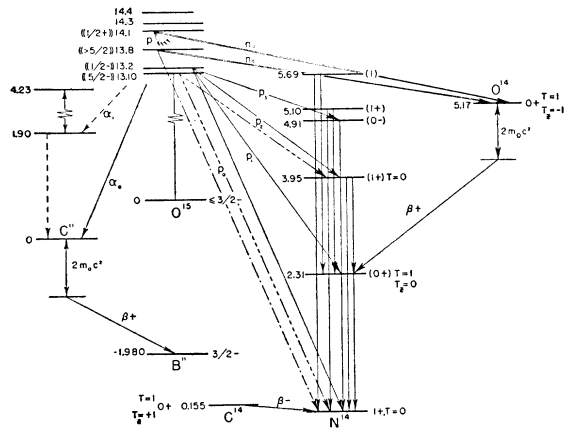

FIG. 9. Schematic diagram showing the levels involved in these experiments together with some of the transitions studied. Excitation energies are given in Mev; J, π, and T values are shown where available. The energies on the left of the figure are referred to the C^{11} and O^{15} ground states whereas the remainder are referred to the N^{14} ground state.

has not been studied in detail, observation of the gamma spectra from $C^{12}(He^3,p\gamma)N^{14}$ indicates that at the 1.3-Mev resonance the lowest four states in N^{14} are being fed with approximately equal intensity. No detectable feeding of the first and second excited states has been observed at the 2.1-Mev resonance. Figure 9 shows the levels in N^{14}, O^{15}, and O^{14} involved in these reactions.[11]

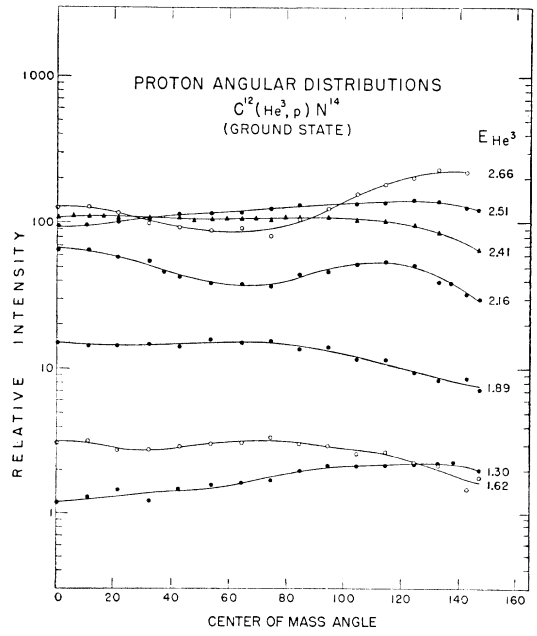

FIG. 10. Angular distributions of protons leading to formation of N^{14} in the ground state. The experimental data have been converted to center-of-mass intensities and angles for this figure and have been normalized to the yield curve of Fig. 8. Note that the ordinate scale is logarithmic. The solid curves are the least-squares fit to the experimental points, and the bombarding energy used is indicated on the right of the figure.

Angular Distributions—$C^{12}(He^3,p)N^{14}$

Angular distributions have been measured at bombarding energies of 1.30, 1.62, 1.89, 2.16, 2.41, 2.51, and 2.66 Mev for each of the three proton groups described above. Figures 10, 11, and 12 show these angular distributions converted to the center-of-mass system and in each case normalized to the 90° excitation curve of Fig. 8. All of these distributions have been fitted to Legendre polynomial expansions of the form

$$d\sigma/d\omega = A[\sum_{n=0}^{L} a_n P_n(\cos\theta)],$$

using a least-squares fitting procedure on the FERUT computer at the University of Toronto. The coefficients

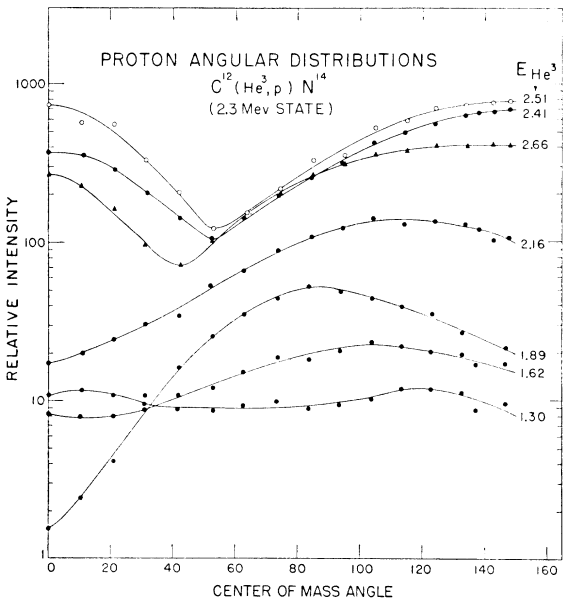

FIG. 11. Angular distributions of protons leading to the formation of N^{14} in its first excited state.

for these expansions with their standard deviations are listed in Table I. In many instances these curves have been fitted with varying values of L (the order of the highest polynomial considered), and, as might be expected, it is found that unless the number of points measured experimentally is at least three times the order of the highest Legendre polynomial used in the expansion, the results obtained by the fitting procedure are not reliable, particularly since the measured data do not extend beyond a laboratory angle of 145°.[18] To investigate this behavior, several of the angular distributions have been fitted with maximum polynomial orders of up to and including 4, 6, 8, and 10. The synthesized curves corresponding to these fits are all quite satisfactory in the angular range 0 to 145°;

[18] D. J. Behrens, Atomic Energy Research Establishment, Harwell Report A.E.R.E. T/R 629, 1951 (unpublished).

TABLE I. Coefficients of the Legendre polynomial expansion least squares fitted to the center-of-mass proton angular distributions in the $C^{12}(He^3,p)N^{14}$ reaction.

Reaction	E_{He^3}	a_0	a_1	a_2	a_3	a_4	a_5	a_6
$C^{12}(He^3,p_0)N^{14}$	2.66	1.00±0.02	−0.56±0.06	0.24±0.08	0.34±0.10	−0.18±0.09	0.08±0.09	0.00±0.07
	2.51	1.00±0.01	−0.08±0.02	−0.21±0.02	0.14±0.02	−0.15±0.03	0.08±0.03	−0.07±0.03
	2.41	1.00±0.01	0.24±0.01	−0.26±0.02	0.20±0.02	−0.06±0.02	0.04±0.02	−0.04±0.02
	2.16	1.00±0.01	0.13±0.04	−0.11±0.05	0.52±0.06	0.03±0.06	−0.08±0.07	0.04±0.05
	1.89	1.00±0.02	0.34±0.04	−0.19±0.06	−0.07±0.07	0.04±0.07	0.02±0.08	0.03±0.07
	1.62	1.00±0.02	0.28±0.05	−0.24±0.07	−0.03±0.08	0.06±0.09	0.02±0.09	0.10±0.08
	1.30	1.00±0.02	−0.21±0.04	−0.22±0.06	0.17±0.07	−0.07±0.07	0.08±0.08	−0.08±0.06
$C^{12}(He^3,p_1)N^{14*}$ (2.3 Mev)	2.66	1.00±0.01	−0.77±0.03	0.05±0.04	0.24±0.05	0.29±0.04	0.05±0.04	0.11±0.03
	2.51	1.00±0.03	−0.70±0.08	0.50±0.11	0.55±0.14	0.16±0.14	0.12±0.16	0.02±0.13
	2.41	1.00±0.01	−0.86±0.02	0.43±0.03	0.33±0.04	0.08±0.04	0.09±0.04	−0.02±0.04
	2.16	1.00±0.02	−0.56±0.04	−0.51±0.06	0.31±0.07	−0.03±0.08	0.02±0.08	−0.04±0.07
	1.89	1.00±0.02	−0.17±0.04	−0.92±0.06	−0.05±0.07	0.15±0.07	0.06±0.08	−0.03±0.07
	1.62	1.00±0.02	−0.33±0.04	−0.37±0.06	0.09±0.07	0.07±0.07	−0.06±0.08	0.08±0.07
	1.30	1.00±0.03	−0.04±0.07	−0.03±0.09	0.22±0.11	−0.05±0.11	−0.02±0.13	0.09±0.10
$C^{12}(He^3,p_2)N^{14*}$ (3.9 Mev)	2.66	1.00±0.02	0.07±0.05	0.91±0.07	1.08±0.09	0.38±0.09	0.14±0.10	0.15±0.09
	2.51	1.00±0.07	0.01±0.17	1.16±0.23	0.68±0.28	0.14±0.30	0.04±0.34	0.12±0.29
	2.41	1.00±0.05	−0.49±0.12	0.36±0.16	0.04±0.19	0.57±0.20	−0.24±0.23	0.35±0.18
	2.16	1.00±0.02	−0.67±0.05	0.87±0.07	0.12±0.09	−0.01±0.09	−0.11±0.11	0.06±0.09
	1.89	1.00±0.01	−0.83±0.03	0.15±0.04	0.20±0.05	0.09±0.05	−0.08±0.05	0.03±0.05
	1.62	1.00±0.02	0.05±0.04	0.10±0.06	0.50±0.07	0.18±0.08	−0.12±0.09	0.08±0.08
	1.30	1.00±0.05	0.24±0.11	−0.38±0.18	0.55±0.18	0.00±0.19	0.15±0.21	−0.30±0.20

however, only those corresponding to maximum orders of 4 and 6 provide reasonable extrapolations of the experimental data beyond 145°. Those corresponding to the higher maximum orders indicate very large negative intensities at 180° and are meaningless. On the basis of these findings, the fits have been restricted to include only up to $P_6(\cos\theta)$ as shown in Tables I and II, and the computer program has been changed to provide for an automatic check synthesis of the fitted curve in the angular region beyond the experimental points.

Excitation Curves—$C^{12}(He^3,n)O^{14}$

Figure 13 shows the corresponding excitation curves at 0° and 90° as well as the 0° counter ratio for the neutrons from the $C^{12}(He^3,n)O^{14}$ reaction. The neutron yield was determined at bombarding energy intervals of approximately 22.5 kev, and the absolute cross sections shown on the ordinate were determined by comparison with the proton yield from the (He^3,p) reaction as will be described in the following section.

The proton gyromagnetic resonance frequency corresponding to the reaction threshold has been determined several times, both by observation of the direct 0° neutron yield and by use of the counter-ratio technique mentioned above. Figure 14 is a typical expanded plot of the 0° yield in the region of the threshold. When converted to He^3 energy using the calibration discussed in the previous section, the threshold energy referred to the $Li^7(p,n)$ calibration is 1449.0±3 kev, whereas, based on the $Li^7(\alpha,\gamma)B^{11}$ calibration point, it is 1450.1±4 kev. It would seem reasonable that the best value for our threshold measurement is then 1449.6±2.8 kev, which is the weighted mean of these two determinations. Any systematic errors, involving, for example, uncertainty as to the exact shape of the yield curve at threshold, would be in the direction to reduce this threshold energy, but at most by the order of 1 or 2 kev. The only previously reported measurement of this threshold is a preliminary one due to Butler,[4] who finds a threshold energy of 1435 kev.

There is evidence in the 90° excitation curve for the 2.1-Mev resonance as well as for the strong resonance in the vicinity of 2.5 Mev and for the higher resonances observed both in the proton excitation curves and by the Naval Research Laboratory group.[19] The counter ratio remained constant through these resonances as

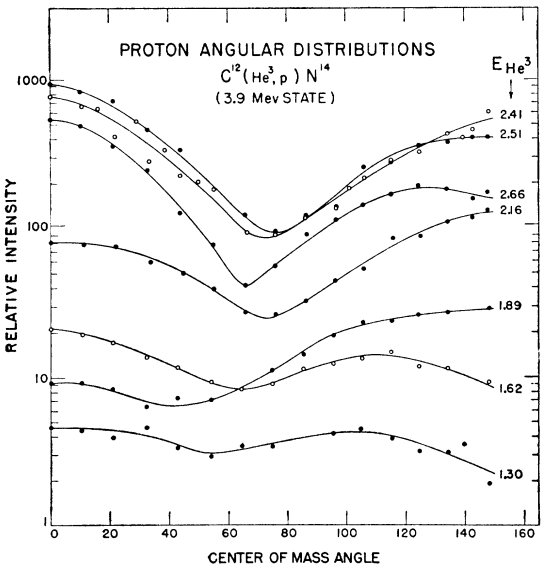

FIG. 12. Angular distributions of protons leading to the formation of N^{14} in its second excited state.

[19] E. H. Geer (private communication).

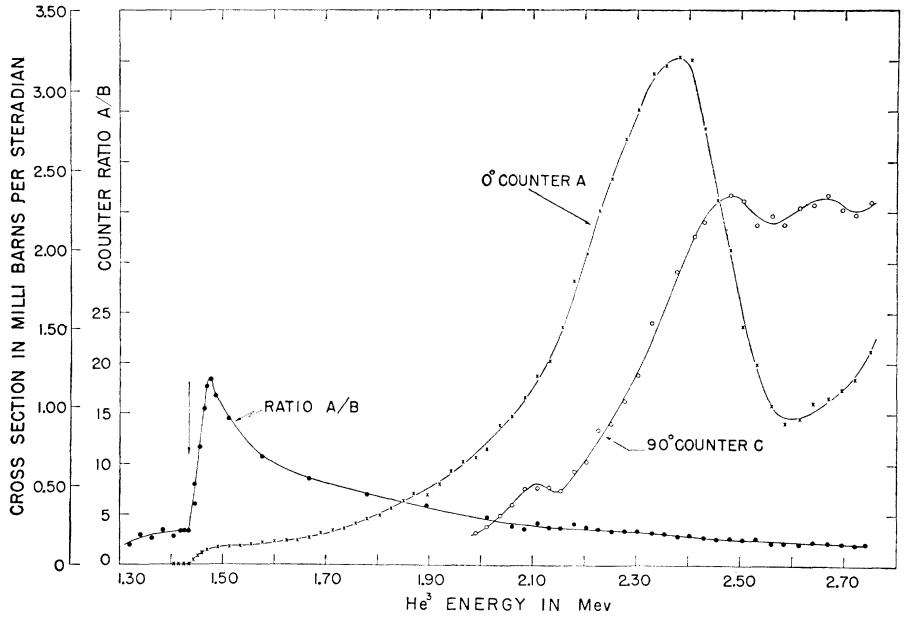

FIG. 13. Neutron yield and counter ratio for the reaction $C^{12}(He^3,n)O^{14}$ as a function of the He^3 bombarding energy. The threshold energy is 1449.6±2.8 kev. The letters A, B, and C refer to the counters so indicated in Fig. 3.

expected; in agreement with the work of Ajzenberg,[20] there is no evidence for low-lying states in O^{14} which would give rise to breaks in this ratio.

Angular Distributions—$C^{12}(He^3,n)O^{14}$

Angular distributions of these neutrons have been measured, using the method previously described, for He^3 bombarding energies of 1.89, 2.16, 2.40, and 2.51 Mev. At these bombarding energies, only neutrons corresponding to the formation of O^{14} in its ground state are possible, and a small, experimentally determined background resulting from neutron scattering from surroundings and from small amounts of neutron production from stray beams striking apertures, etc., in the beam tube has been subtracted. By minimizing the amount of matter in the vicinity of the target, the contribution from scattered neutrons has been kept small and is, in all cases, less than 15%. The directional sensitivity of the long counter was useful in this respect.

The angular distributions thus obtained, converted to the center-of-mass system and normalized to the yield curves of Fig. 13, are shown in Fig. 15. The small correction proportional to the second derivative of the distribution arising from the finite acceptance angle of the detector has not been applied to these data and is negligible because of the small values for this derivative. Table II lists the coefficients a_n in the corresponding Legendre polynomial expansions.

Relative Cross Sections—$C^{12}(He^3,p_1)N^{14*}$ and $C^{12}(He^3,n_0)O^{14}$

Since the O^{14} ground state and the 2.3-Mev state of N^{14} are members of an isobaric triplet, it was of particular interest to study the relative cross sections for the formation of these states from the decay of common states in the compound nucleus O^{15}. Because these reactions proceed to analog final states, the ratio of the cross sections is given simply by

$$\frac{\sigma(He^3,p)}{\sigma(He^3,n)}=\left[\frac{\langle T_1T_2T_{1z}T_{2z}|T_1T_2TT_z\rangle}{\langle T_1'T_2'T_{1z}'T_{2z}'|T_1'T_2'TT_z\rangle}\right]^2, \quad (1)$$

where T_1 = isobaric spin of the residual nucleus, T_2 = isobaric spin of the outgoing particle, and T = isobaric spin of the compound state = isobaric spin of the incident particle for $T=0$ targets. Substituting the appropriate values from Fig. 9, this results in $\sigma(He^3,n_0)=2\sigma(He^3,p_1)$. It would be expected that this would be the case somewhat above the neutron threshold in the reactions considered here.

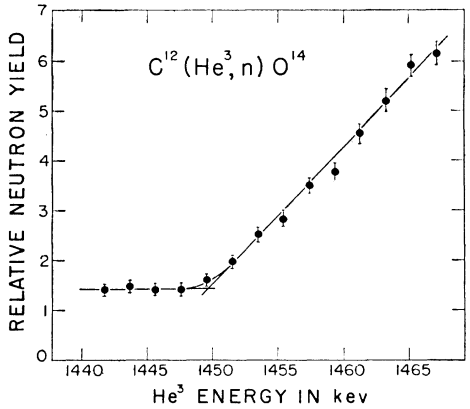

FIG. 14. Typical neutron excitation curve in the region of the $C^{12}(He^3,n)O^{14}$ threshold.

[20] F. Ajzenberg and W. Franzen, Phys. Rev. 94, 409 (1954).

TABLE II. Coefficients of the Legendre polynomial expansion least squares fitted to the center-of-mass neutron angular distributions in the $C^{12}(He^3,n)O^{14}$ reaction.

Reaction	E_{He^3}	a_0	a_1	a_2	a_3	a_4	a_5	a_6
$C^{12}(He^3,n_0)O^{14}$	2.51	1.00±0.01	−1.13±0.03	0.42±0.05	0.08±0.06	0.13±0.06	−0.12±0.06	0.15±0.05
	2.41	1.00±0.01	−0.63±0.02	0.46±0.03	0.13±0.04	0.03±0.04	0.02±0.04	0.01±0.03
	2.16	1.00±0.06	0.28±0.14	0.09±0.19	0.08±0.24	−0.05±0.24	0.17±0.28	−0.10±0.24
	1.89	1.00±0.05	−0.16±0.10	0.15±0.13	−0.27±0.16	0.15±0.17	−0.02±0.22	0.00±0.20

As shown in Fig. 9, the β^+ decay of O^{14} proceeds through the 2.3-Mev level in N^{14}; the 2.3-Mev radiation observed during He^3 bombardment of C^{12} results therefore from three separate sources: (a) direct feeding by the P_1 proton group to the 2.3-Mev level in the $C^{12}(He^3,p)N^{14}$ reaction; (b) cascade de-excitation of higher levels in N^{14}, formed in the same reaction, through the level at 2.3 Mev; and finally (c) the β^+ decay of O^{14} produced by the $C^{12}(He^3,n)O^{14}$ ground-state reaction.

Since only the ground-state (He^3,n) reaction is energetically possible on carbon at the bombarding energies used and since the partial branching ratios of the higher levels in N^{14} for decay through that at 2.3 Mev are known as discussed below, a determination of the relative yield of 2.3-Mev radiation, first with the beam on target and second with it interrupted mechanically, so that only gamma rays following the O^{14} β^+ decay occur, allows the calculation of the ratio of the (He^3,n_0) and (He^3,p_1) cross sections. In particular, this somewhat involved procedure avoids the necessity for direct measurement of the efficiency of the neutron detectors as well as correction for the neutron backgrounds. The cross sections determined here were in fact used to compute the neutron-counter efficiencies previously quoted.

If He^3 bombardment of the carbon target is continued until secular equilibrium is established, then the measured yield of 2.3-Mev radiation during a run of length

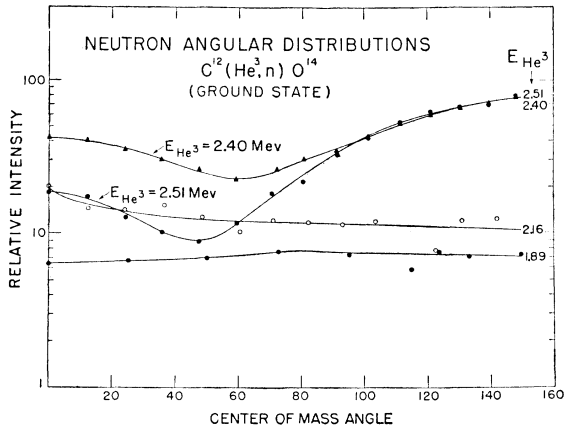

FIG. 15. Angular distributions of neutrons from the reaction $C^{12}(He^3,n_0)O^{14}$. The experimental data have been converted to center-of-mass intensity and angle and have been normalized to the excitation curves of Fig. 14. Note that the ordinate scale is logarithmic.

T_0 is given by

$$N=ADT_0\epsilon[\sum_{r=1}^{R} b_r\sigma_r+\sigma_n], \tag{2}$$

where A is the flux of incident He^3 ions, D is the areal density of the target in atoms/cm², ϵ is the efficiency of the gamma detector for 2.3-Mev radiation, σ_r is the total cross section for the $C^{12}(He^3,p_r)N^{14}$ reaction leading to the rth excited level, b_r is the fractional branching ratio for the decay of this level through that at 2.3 Mev, and σ_n is the total cross section for the $C^{12}(He^3,n)O^{14}$ ground state reaction. Furthermore, if, after equilibrium is established, the beam is interrupted mechanically and after an interval T_1 the yield of 2.3-Mev radiation is measured for a time T_2, this yield is

$$N'=(AD\epsilon\sigma_n/\lambda)e^{-\lambda T_1}(1-e^{-\lambda T_2}), \tag{3}$$

where the notation is as in Eq. (2) and λ is the radioactive decay constant for O^{14}.

For bombarding energies up to 2.0 Mev, examination of the direct gamma spectrum associated with He^3 bombardment of carbon shows no detectable feeding of any state in N^{14} higher than the fourth at 5.1 Mev[11]; consequently R in Eq. (2) is limited to 4 in this range. Clearly $b_1\equiv 1$, and the work of Woodbury, Day, and Tollestrup[21] gives $b_3\approx 0$ and $b_4\approx 26\%$.

A previously reported measurement from this laboratory[1] gave $b_2=(95.7\pm0.8)\%$. In determining this value, measurements were made with the proton detector fixed at 90° and the gamma detector at 0° and 90° to the beam in the plane defined by the beam and proton detector. Further measurements have been carried out to check on the possibility of an azimuthal correlation as well, in that the gamma radiation in coincidence with the P_2 proton group has been examined by rotating the proton detector through 90° from its previous position and examining the gamma radiation at 90° and 0° to the beam in a plane perpendicular to the axis of the proton detector. As in the previously reported case, there is a slight indication of a $P_2(\cos\theta_\gamma)$ correlation term, but to within the statistical accuracy of the measurements this term is negligible, and the weighted mean of the branching ratios for direct decay determined at 0° and at 90° in the perpendicular plane is $(3.1\pm0.8)\%$, to be compared with the previous value, in the proton detector plane, of $(4.3\pm0.8)\%$. It is reasonable to conclude that the best value for this branching ratio is the weighted mean of these separate

[21] Woodbury, Day, and Tollestrup, Phys. Rev. **92**, 1199 (1953).

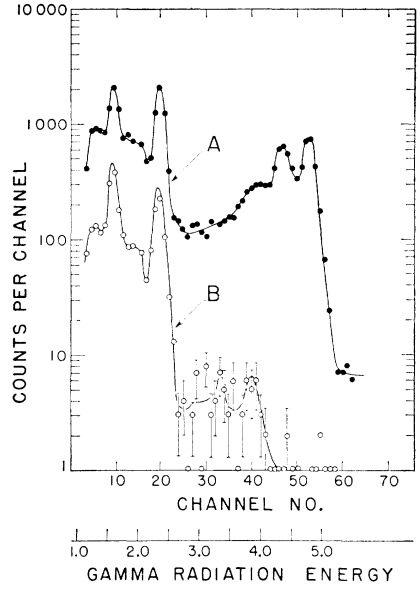

FIG. 16. Gamma spectra from $C^{12}(He^3,p\gamma)N^{14}$ at $E_{He^3}=1.3$ Mev. Curve A is the direct spectrum showing the 1.64-, 2.31-, and 4.91-Mev radiation. Curve B is the spectrum in coincidence with the proton group P_2 to the 3.9-Mev state in N^{14} showing the weak 3.9-Mev direct transition. Note the absence of 1.90-Mev radiation which would result from de-excitation of the first excited state of C^{11} produced in the $C^{12}(He^3,\alpha)C^{11}$ reaction.

determinations, equal to $(3.7\pm0.6)\%$, to be compared with the theoretical predictions[22] of 3.9% due to Visscher and Ferrell and of $\sim1\%$ due to Elliott.

In addition to the partial branching ratio just noted, correction for the cascade contribution to the yield of 2.3-Mev radiation required that the correlations of the various cascade gammas be determined. The gamma spectrometer efficiencies were determined directly by observation of the gamma spectrum in coincidence with the P_2 proton group as shown in Fig. 16(B). Figure 16(A) is the direct spectrum for comparison, showing the 4.9-Mev radiation from the third excited state which masks the 3.7% direct 3.9-Mev transition shown in Fig. 16(B). The spectrometer efficiency is given directly by the ratio of the number of coincidence

TABLE III. Analysis of the spectra shown in Fig. 17. α is the coefficient of the $P_2(\cos\theta_\gamma)$ term in the corresponding angular distribution, and the relative radiation yields are determined from the observed counts, the known branching ratios, the spectrometer efficiencies, and the measured distributions. These are arbitrarily normalized to 1.00 for the 2.79-Mev radiation.

Gamma energy Mev	Counts in total absorption peak 0°	90°	α	Gamma spectrometer efficiency %	Relative radiation yield
1.64	2046±50	1502±50	0.22±0.02	0.92±0.05	1.64
2.31	5568±100	5348±100	0	0.80±0.05	5.71
2.79	922±30	413±20	0.55±0.05	0.70±0.05	1.00

[22] W. M. Visscher and R. A. Ferrell, University of Maryland Physics Department Technical Report No. 19, September, 1955 (unpublished), and private communication; J. P. Elliott, Phil. Mag. **6**, 503 (1956).

counts in a given energy peak to the corresponding number of proton counts after correction for the measured correlations and is listed in Table III. Since only states of angular momentum 1 or 0 are involved,[11] the angular distributions can at most have the form

$$w(\theta)=w_0[P_0(\cos\theta_\gamma)+\alpha P_2(\cos\theta_\gamma)]$$

and measurement of the spectra at $\theta_\gamma=0°$ and 90° is sufficient to determine α and consequently the averaged relative yields. These quantities are listed in Table III for a He^3 bombarding energy of 2.0 Mev. Figure 17(A) is a typical spectrum measured at $\theta_\gamma=0°$ and Fig. 17(B) the corresponding spectrum at $\theta_\gamma=90°$, from which the data of Table III were obtained. The weak radiation at 2.79 Mev is the cascade from the state at 5.10 Mev through that at 2.31 Mev; that at 1.64 Mev is the corresponding cascade from the 3.95-Mev level. Figure 17(C) is the spectrum obtained with the beam interrupted mechanically and results purely from the de-excitation of the O^{14} ground state by β^+ decay via the 2.3-Mev level in N^{14}. The experimental counts so obtained have been corrected for background and for the underlying tails of higher energy gamma radiations using measured standard spectral shapes. To obtain the values of σ_r/σ_1 for $r=2, 3, 4$, the measured angular distributions were integrated, normalized to the 90° yield of Fig. 8, and combined with the data of Table III.

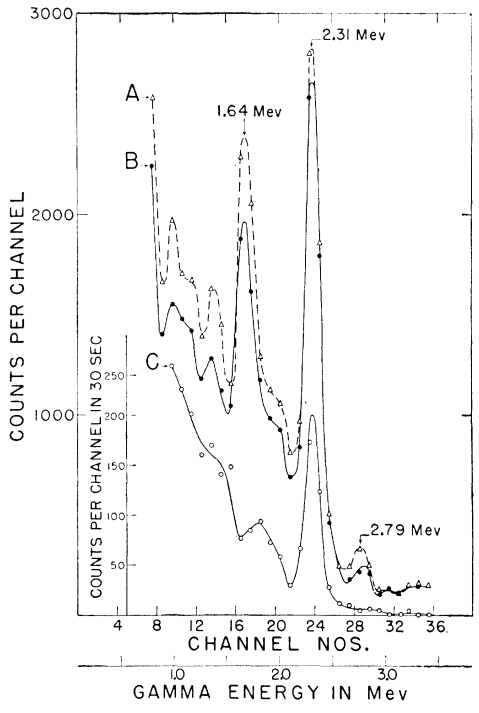

FIG. 17. Gamma spectra from $C^{12}(He^3,p\gamma)N^{14}$ at $E_{He^3}=2.0$ Mev. Curve A is obtained with the beam on target and the gamma detector at 0° to the beam axis. Curve B is obtained with the beam on target and the gamma detector at 90° to the beam axis. Curve C is obtained with the beam interrupted mechanically and is associated with the β^+ decay of O^{14}.

These values may then be substituted into Eq. (4):

$$\frac{\sigma_n}{\sigma_1}=K\left\{\frac{N}{N'}\left(\frac{e^{-\lambda T_1}(1-e^{-\lambda T_2})}{\lambda T_0}\right)-1\right\}^{-1}, \qquad (4)$$

which is obtained by combining Eqs. (2) and (3), where N and N' are the number of counts in the 2.31 Mev gamma radiation full absorption peak with the beam on and off the target for periods T_0 and T_2, respectively, K is a function of the b_r and σ_r, and is constant for any particular bombarding energy. At 2.0 Mev, $K=3.048$. The average of several such determinations at 2.0 Mev is $\sigma_n/\sigma_1=0.89$, and the different measurements do not vary from this by more than about eight percent, which is within the order of accuracy claimed for this measurement.

As a check that the 2.3-Mev radiation observed after interruption of the beam was in fact associated with the $O^{14}(\beta^+)$ decay, a rough lifetime measurement was carried out. The results shown in Fig. 18 indicate a half-life of 72 sec in excellent agreement with the value of 72.1 ± 0.4 sec quoted for O^{14}.[23]

Having established the ratio of the (He^3,n) and (He^3,p) cross sections at 2.0 Mev, the ratio at other energies was obtained by integrating the measured angular distributions for both protons and neutrons, normalizing to the yield curves shown in Figs. 8 and 13, and finally normalizing the ratio of the total cross sections thus determined to the ratio at 2.0 Mev. The efficiency of the neutron detectors has been assumed to be independent of energy. The points so obtained are shown as closed circles in Fig. 19, which is a plot of the ratio $\sigma(He^3,n_0)/\sigma(He^3,p_1)$ as a function of the He^3 bombarding energy. As shown in Figs. 11 and 15 and as will be discussed in the following section, the angular distributions of the protons to the 2.3-Mev state of N^{14} and of the neutrons to the O^{14} ground state are quite similar, particularly at the higher bombarding energies. The triangular points of Fig. 19 were obtained therefore by forming the ratio of the 90° differential cross sections and normalizing this to the determined ratio in the region of 2.0 Mev. This allows determination of the ratio at energies where the angular distributions were not measured.

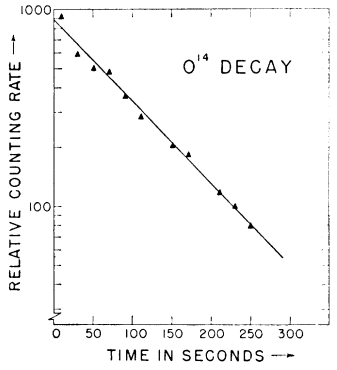

FIG. 18. O^{14} β^+-decay lifetime check. The line drawn on the figure corresponds to a half-life of 72 seconds.

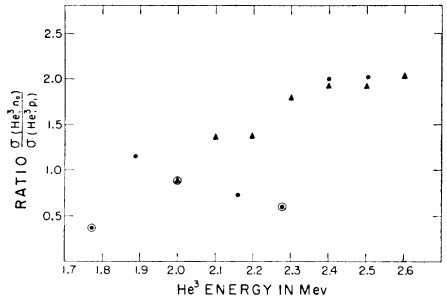

FIG. 19. Ratio of the $C^{12}(He^3,n_0)O^{14}$ to $C^{12}(He^3,p_1)N^{14*}$ cross sections as a function of bombarding energy. The double circled points represent detailed measurements as described in the text; the closed circles were obtained by integrating the corresponding angular distributions and the triangular points by comparison of the 90° differential cross sections.

Detailed measurements of the relative cross sections of the sort described here for 2.0 Mev have also been made for energies of 1.78 Mev and 2.28 Mev. These points and that at 2.0 Mev are shown in Fig. 19 as double circles. The expressions which have been used in these determinations will of course not apply when the bombarding energy becomes sufficiently high to excite appreciably higher levels than the fourth in N^{14} without addition of higher terms in the $\Sigma_r b_r\sigma_r$ factor. This effect is quite pronounced for the He^3 bombarding energy of 2.28 Mev, where the calculated ratio is $\sigma_n/\sigma_1=0.6$, indicating large contributions to the yield of 2.3-Mev radiation from cascade de-excitation of higher states, primarily from that at 5.69 Mev, which is quoted[21] as having a 65% branch to the state at 2.3 Mev. This is shown quite clearly in Fig. 19, where the 2.28-Mev point is low.

Relative Cross Sections—$C^{12}(He^3,\alpha_0)C^{11}$ and $C^{12}(He^3,n_0)O^{14}$

At He^3 energies below 2.0 Mev the $C^{12}(He^3,\alpha)C^{11}$ reaction can feed only the ground and first excited states of C^{11}. Furthermore, examination of the gamma spectra such as are shown in Figs. 16 and 17 shows no detectable 1.90-Mev radiation which would result from de-excitation of the first excited state in C^{11}, leading to the conclusion that, owing to barrier effects, effectively only the ground state reaction has an appreciable cross section. By studying the decay of the 0.511-Mev annihilation radiation from $C^{11}(\beta^+)B^{11}$ and $O^{14}(\beta^+)N^{14}$ following interruption of the He^3 beam, it is therefore possible to obtain the ratio of the ground state $C^{12}(He^3,\alpha)C^{11}$ and $C^{12}(He^3,n)O^{14}$ reaction cross sections since the Q value of -3.55 Mev insures no contribution from N^{13} formed in the $C^{12}(He^3,d)N^{13}$ reaction. The upper curve in Fig. 20 shows the decay of this radiation following a 120 minute bombardment with 2.0-Mev He^3 ions. The straight line corresponds to a half-life of 20.5 minutes, identifying this component as due to the decay

[23] J. B. Gerhart, Phys. Rev. **95**, 288 (1954).

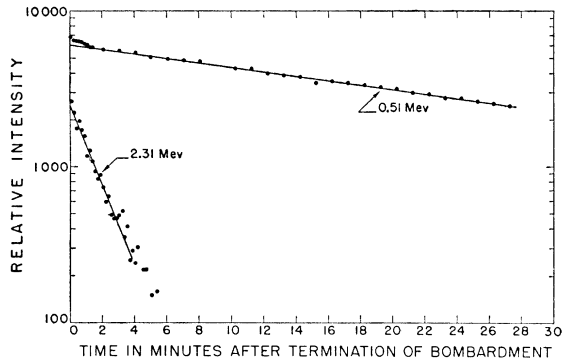

FIG. 20. Radiation associated with the decay of O^{14} and C^{11} produced by the $C^{12}(He^3,n)O^{14}$ and $C^{12}(He^3,\alpha)C^{11}$ reactions, after mechanical interruption of the He^3 beam. The lines drawn on the figure correspond to half-lives of 72 seconds and 20.5 minutes, respectively. The He^3 bombarding energy was 2.0 Mev. Formation of N^{13} in the $C^{12}(He^3,d)N^{13}$ reaction is not energetically possible at this bombarding energy.

of C^{11}.[11] The rise, immediately after the end of bombardment, above this line results from the 72.1 second O^{14} activity. Since the He^3 beam intensity was maintained constant to within a few percent during the bombardment, the cross section ratio is given by

$$\frac{\sigma(He^3,\alpha_0)}{\sigma(He^3,n_0)}=\frac{N_0(C^{11})}{N_0(O^{14})}\left(\frac{1-\exp[-\lambda(O^{14})T]}{1-\exp[-\lambda(C^{11})T]}\right), \quad (5)$$

where N_0 represents the counting rate extrapolated back to the end of bombardment and T is the duration of bombardment.

Because of the inaccuracy inherent in obtaining $N_0(O^{14})$ as the difference of two comparatively large numbers, the relative efficiency of the gamma spectrometer for 0.51- and 2.31-Mev radiation was measured by bombarding a clean target for 75 seconds and examining these radiations simultaneously after this bombardment. The ratio of the efficiencies was found to be 2.7; consequently the yield of 0.51-Mev radiation from the O^{14} decay may be obtained directly from that of the 2.31-Mev radiation, which in turn can be measured with considerably greater accuracy. The lower curve in Fig. 20 shows the decay of this radiation obtained simultaneously with that for the 0.51-Mev radiation.

With a bombarding energy of 2.0 Mev, the ratios found are 10.0 and 6.0, depending upon whether only the 0.51 or both 0.51- and 2.31-Mev data are used in the calculation. Corresponding ratios for a bombarding energy of 1.78 Mev are 11.1 and 8.3. As noted previously, the second of these ratios in each case is considered more reliable. It should be emphasized that this measurement is not intended to be a precise one; the method is quite sensitive to target changes during bombardment and to beam intensity fluctuations, particularly during the latter part of the bombardment. A weighted mean of the above data would then give $\sigma(He^3,\alpha_0)/\sigma(He^3,n_0)=7.3$ and 9.2 at bombarding energies of 2.0 and 1.78 Mev. These ratios are estimated to have an error of ± 3.0.

A more accurate determination of the (He^3,α) cross section will be carried out using an ionization chamber of known efficiency to detect the alpha particles directly.

Absolute Cross-Section Determination—$C^{12}(He^3,p)N^{14}$

Having obtained a value for the relative cross sections of the (He^3,n_0) to (He^3,p_1) and of the (He^3,α_0) to (He^3,n_0) reactions, it was sufficient only to determine the absolute cross section for the $C^{12}(He^3,p)N^{14}$ reactions. Two separate measurements of the efficiency of the proton counter have been used in making this absolute cross-section determination. The target thickness was determined as described previously, and the beam current integrator was calibrated by comparison with a precision electrometer system. The facts that 99% He^3 has been used in the accelerator ion source for these measurements and that this accelerator has never been used with either deuterium or tritium make it possible to determine the actual He^3 ion flux on target by a direct integration. With source gas of lower isotopic purity or where appreciable deuterium or tritium has been absorbed on the accelerator surfaces, auxiliary measurements to determine the amount of HD^+ and T^+ contaminants in the beam would be required. In the first series of measurements, the efficiency of the proton counter was computed from the measured geometry as shown in Fig. 1. Measurements taken with detector efficiencies differing by a factor of two (obtained by withdrawing the photomultiplier and aperture system by measured amounts) agree to within 6%. The data have a 1.5% statistical uncertainty and the efficiency calculations an estimated 5% error. Consequently, this agreement is considered as satisfactory. The absolute differential cross sections thus obtained are on the ordinates of the excitation curves in Figs. 8 and 13. In Table IV the total cross sections for the reactions are listed for the energies at which angular

TABLE IV. Total cross sections in millibarns for the $C^{12}(He^3,p)N^{14}$ and $C^{12}(He^3,n_0)O^{14}$ reactions. These have been obtained by integration of the angular distributions. The approximate $C^{12}(He^3,\alpha_0)C^{11}$ reaction cross sections have been obtained by comparison with those for the $C^{12}(He^3,n_0)O^{14}$ reaction.

Bombarding energy in Mev	1.30	1.62	1.89	2.16	2.41	2.51	2.66
Reaction							
$C^{12}(He^3,p_0)N^{14}$	0.026	0.30	1.7	5.2	13	16	18
$C^{12}(He^3,p_1)N^{14*}$ (2.3 Mev)	0.038	0.59	1.2	3.5	17	17	13
$C^{12}(He^3,p_2)N^{14*}$ (3.9 Mev)	0.024	0.90	1.7	6.1	25	25	14
$C^{12}(He^3,n_0)O^{14}$			2.0	7.9	34	34	
$C^{12}(He^3,\alpha_0)C^{11}$		~20 at 1.78 Mev	~50 at 2.0 Mev				

distributions have been measured in the case of the (He^3,p) and (He^3,n) reactions and at 1.78 and 2.0 Mev for the (He^3,α) reaction. The errors in these cross sections are estimated at 10% for the first two reactions and 30% for the last.

A second determination of the proton counter efficiency was obtained by an examination of the proton spectrum in coincidence with the 2.3-Mev radiation. This measurement was carried out at low energy (1.30 Mev), below the $C^{12}(He^3,n)O^{14}$ threshold; consequently none of the observed 2.3-Mev radiation resulted from the O^{14} beta decay. The absence of detectable 2.79-Mev radiation from the 5.1-Mev level in N^{14} in the spectra shown in Fig. 21 also indicates that at this energy at most a negligible fraction of the 2.31-Mev radiation resulted from the de-excitation of states in N^{14} other than those at 2.31 and 3.95 Mev. Part *C* of this figure shows, first, a direct spectrum, showing the 1.64- and 2.31-Mev radiation from these two levels. Inset and shaded-in part *C* of the figure is the spectrum obtained by self-gating the spectrum in coincidence with a voltage gate set on the 2.3-Mev full absorption peak as described previously. This provides a direct check on the setting of this gate. Part *A* of the figure shows the direct proton spectrum, while part *B* shows that in coincidence with the 2.3-Mev gate just described. The residual yield of the P_0 group is due to accidental coincidences, since the coincidence circuits readily available were slow, having resolving times of the order of 1 μsec. Since, as noted previously, the angular correlation of the 2.31-Mev radiation is isotropic, no correction is required for this correlation here. In obtaining the total yields of the P_1 and P_2 proton groups from the measurements at 90°, the angular distributions shown in Figs. 11 and 12 have been integrated and normalized to the experimental counting rate at 90°. It should perhaps be remarked that only when the gamma ray in an (a,$b\gamma$) reaction comes from a $J=0$ state are the triple and double correlations of the b particles identical, which justifies this use of these double correlation angular distributions in this triple correlation measurement.[24] From these measurements the efficiency of the proton counter, ϵ_2, is given by the ratio of the corrected number of counts in the P_1 and P_2 peaks in the coincidence spectrum to the number of 2.3-Mev radiation counts in the gate where, in correcting the proton counts, the yields have been averaged over the distributions, and the ~4% branch of the 3.9-Mev state de-excitation directly to the ground state[1] has been subtracted. The efficiency of the proton counter as determined in this way agrees to within 3% with the value computed from the measured dimensions. The mean of these determinations gives an efficiency of 0.067%.

[24] Sharp, Kennedy, Sears, and Hoyle, Chalk River Report CRT-556, 1954 (unpublished).

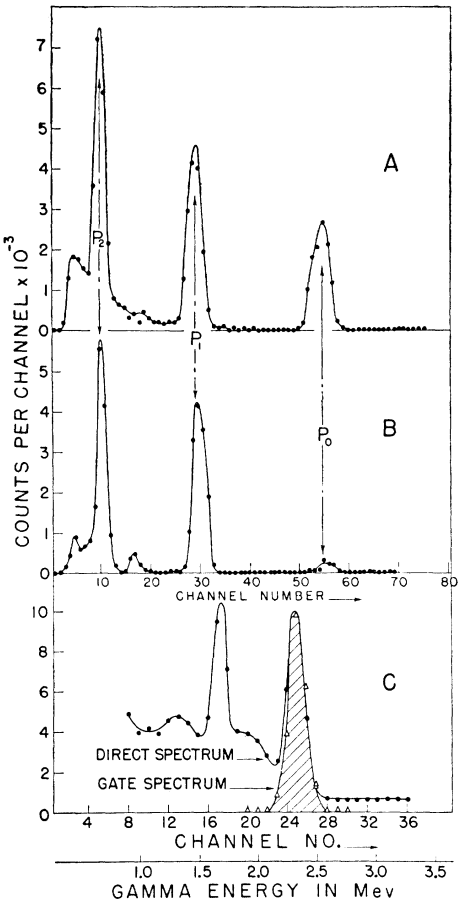

FIG. 21. Curve *A* is a direct proton spectrum from the $C^{12}(He^3,p)N^{14}$ reaction obtained at a bombarding energy of 1.3 Mev. Curve *C* shows the corresponding gamma-radiation spectrum and, superimposed, the spectrum of the radiation which opens a voltage gate set on the 2.3-Mev gamma. Curve *B* is the proton spectrum in coincidence with the pulses in this gate. The cutoff in the low channels is instrumental and is used to limit the kicksorter input to the spectrum region of interest.

High-Energy Gamma Radiation

In examining the higher energy gamma radiation spectra associated with He^3 bombardment of natural carbon targets, a relatively strong gamma ray of 15 Mev is seen, presumably from the first $T=1$ state in C^{12} at 15.09 Mev[11] excited in the $C^{13}(He^3,\alpha\gamma)C^{12}$ reaction. A detailed study of this radiation as well as that from neighboring states in C^{12} has been carried out using separated isotopic targets of C^{13} and B^{10} and the reactions $C^{13}(He^3,\alpha\gamma)C^{12}$ and $B^{10}(He^3,p\gamma)C^{12}$. The results will be published in a forthcoming paper.

DISCUSSION

Excitation Curves

The excitation curves for C^{12}, as shown in Figs. 8 and 13, are characterized by the presence of resonance structure in marked contrast to the corresponding

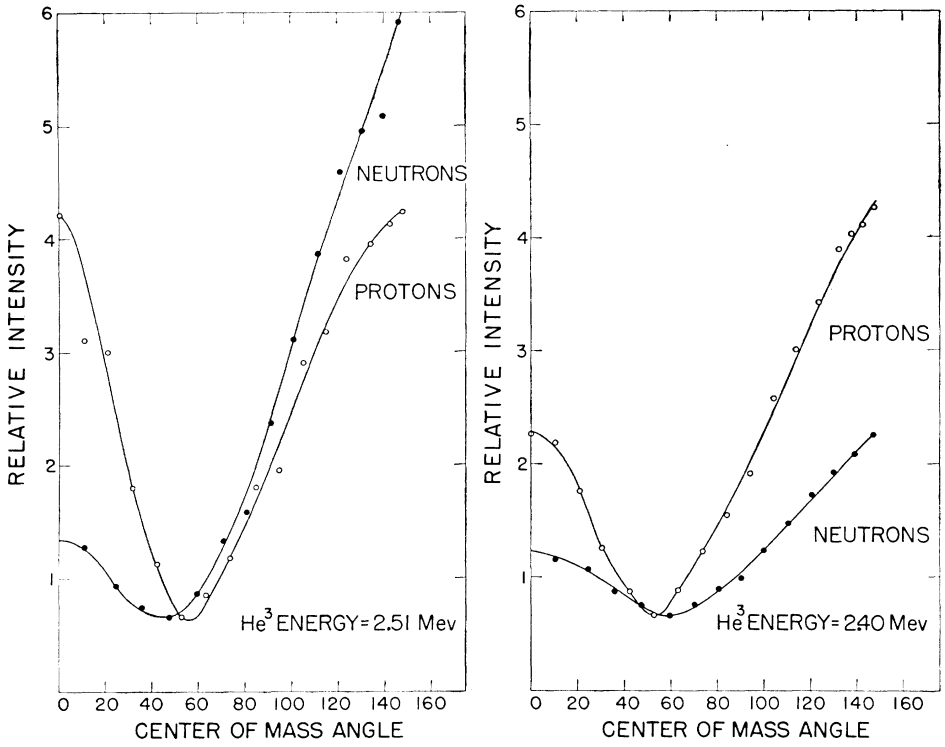

FIG. 22. A comparison of the $C^{12}(He^3,p_0)O^{14}$ and $C^{12}(He^3,p_1)N^{14*}$ angular distributions at the two highest energies studied. The intensities at the minima have been arbitrarily set equal for display purposes.

results for He^3 induced reactions on Be^9,[25] where these curves rise monotonically with energy. In the bombardment of Be^9, the excitation in the compound nucleus, C^{12}, is about 27 to 28 Mev, whereas in the C^{12} bombardments, the excitation in the compound nucleus O^{15} is about 13 to 14 Mev. The levels in O^{15} corresponding to the observed resonances have been listed in the previous section. It is perhaps surprising that an even-even nucleus such as C^{12} should have a sufficiently high level density at an excitation energy of 27 Mev to smear out completely individual level effects as seems to be the case. The measurement interval of about 22.5 kev and the relatively thick targets used in both measurements result in a low detection sensitivity for very narrow, weak resonances.

The fact that the weak resonance at 1.2 Mev observed in the proton distribution feeds only the $1+$, $T=0$ ground and second excited states and not the $0+$ and presumed $0-$ second and fourth excited states is consistent with the assignment of $5/2-$ or $3/2+$ to this resonance. Consideration of the orbital momenta required for transitions to the first four levels in N^{14} and the fact that all four levels are fed with approximately equal intensity at the 1.31-Mev resonance make the assignment of $1/2-$ with s-wave, low-energy protons to the 4.9-Mev state seem most probable. The required orbital momenta and the fact that the 1.2-Mev resonance is considerably weaker than that at 1.3 Mev favor selection of the $5/2-$ assignment noted above for the 1.2-Mev resonance.

The strong yields of protons to the three lowest states of N^{14} and of neutrons to the O^{14} ground state, together with the fact that the yield of 4.9-Mev radiation is relatively low at the 2.52-Mev resonance, suggest the assignment of $1/2+$ to this level on the basis of the above arguments. Nothing further can be said regarding the higher resonances. Work at higher energy has substantiated the existence of a very strong resonance just beyond the energy limit of our machine.[19] There is slight evidence for the appearance of weak, high-energy resonances in the neutron excitation curves as well, but these have not been studied in sufficient detail in this energy region to locate the resonances accurately.

The weak resonance at about 2.15 Mev in the P_0 excitation curve appears as a step in the 90° neutron excitation curve. There is no obvious reason why this should not occur in the P_1 and P_2 curves, but several checks in this energy region have failed to show any evidence for it. A possible explanation is that this is a high spin (greater than 5/2) resonance. It should be emphasized that these assignments are suggested rather than fixed by the arguments listed.

The cross sections as measured for the (He^3,p), (He^3,n), and (He^3,α) reactions are comparable to those for (d,p) reactions for similar energies and targets.[11,26] Since no levels have been observed in O^{14} below an

[25] Almqvist, Bromley, Gove, Litherland, and Paul (to be published).

[26] Bromley, Bruner, and Fulbright, Phys. Rev. **89**, 396 (1953) and unpublished work.

excitation of about 5.5 Mev,[20] the $C^{12}(He^3,n)O^{14}$ reaction constitutes a source of monoergic neutrons from 0 to about 6 Mev. Unfortunately, the low cross section and high associated gamma-radiation flux greatly reduce its potential usefulness for incident He^3 energies below 3 Mev. Since the cross section might be expected to increase rapidly with energy, this reaction may be quite useful with higher He^3 energies.

Analog State Reactions

The ratio of the (He^3,n) and (He^3,p) cross sections to the O^{14} ground state and to the 2.3-Mev level in N^{14} as shown in Fig. 19 is in agreement with the isobaric spin prediction. Since the isobaric spin factors in the predicted cross section are multiplicative and angle independent, the differences in the neutron and proton distributions should be due only to different barrier effects on the emitted nucleons. Since the outgoing protons considered here are at an energy between one and two times the Coulomb barrier, it should be expected that, away from the $C^{12}(He^3,n)O^{14}$ threshold, the angular distributions of the neutrons from this reaction and of the protons from the $C^{12}(He^3,p_1)N^{14*}$ reaction, when corrected to the center-of-mass system of reference, should be similar and that as the energy increases and barrier effects become negligible they should become identical. Figure 22 compares these distributions at the two highest energies at which both were measured, 2.40 and 2.51 Mev. As seen in this figure, there is marked similarity between the curves, and this similarity increases with increasing energy as expected.

Threshold Measurement—$C^{12}(He^3,n)O^{14}$

The measured $C^{12}(He^3,n)O^{14}$ threshold energy of 1449.6 ± 2.8 kev corresponds to a Q value for the ground state reaction of -1158.5 ± 3 kev. This is to be compared with a value of 1166 ± 39 kev calculated from the currently accepted mass values as quoted by Mattauch.[14] This Q value, together with a series of reaction cycles linking C^{12} and N^{14} and the measured excitation of the first excited state in N^{14}, provides a new determination of the mass of O^{14} and of the end point of the O^{14} positron spectrum. Adjusted Q values and tabulated mass defects quoted by Mattauch *et al.*[14] have been used to obtain the mass-defect difference of the N^{14} and C^{12} ground states in the following reaction cycles:

(a) $N^{15}(p,\alpha)C^{12}$, $N^{14}(n,\gamma)N^{15}$—

$$N^{14}-C^{12}=\alpha-d-2.2262(\pm1.3)+4.9622(\pm2.7)+10.8421(\pm4.2)$$
$$=3.4623(\pm6.2);$$

(b) $N^{15}(p,\alpha)C^{12}$, $N^{14}(d,p)N^{15}$—

$$N^{14}-C^{12}=\alpha-d+4.9622(\pm2.7)+8.6159(\pm4.1)$$
$$=3.4623(\pm6.0);$$

(c) $C^{13}(d,p)C^{14}$, $C^{14}(\beta^-)N^{14}$, $C^{12}(n,\gamma)C^{13}$—

$$N^{14}-C^{12}=2n-2.2262(\pm1.3)-4.9474(\pm2.1)-0.1553(\pm1.0)-5.9404(\pm3.4)$$
$$=3.4623(\pm4.7);$$

(d) $C^{12}(d,p)C^{13}$, $C^{13}(d,p)C^{14}$, $C^{14}(\beta^-)N^{14}$—

$$N^{14}-C^{12}=2d-2p-2.7212(\pm1.9)-5.9404(\pm3.4)-0.1553(\pm1.0)$$
$$=3.4625(\pm6.0);$$

(e) $N^{14}(d,\alpha)C^{12}$—

$$N^{14}-C^{12}=13.4780(\pm4.3)+\alpha-d$$
$$=3.4622(\pm5.5);$$

where the defects are listed in Mev and the standard deviations in kev. The weighted mean of these differences is 3.4623 ± 0.0025 Mev.

This difference, coupled with the measurement of the excitation of the first excited state of N^{14} at 2.313 ± 0.005 Mev by Bockelman *et al.*[27] and with the $C^{12}(He^3,n)O^{14}$ Q value of -1158.5 ± 3 kev reported here, requires an end-point energy for the positron spectrum from O^{14} of 1809.7 ± 7.8 kev and a mass defect for O^{14} of 12.146 ± 0.0065 Mev. These are to be compared with the positron end point of 1835 ± 8 kev determined by Gerhart[23] and with a mass defect for O^{14} of 12.153 ± 0.039 Mev quoted by Mattauch *et al.*[14]

This end-point energy is of particular interest since it allows the determination of the ft value for the $0+\rightarrow0+$, $O^{14}(\beta^+)$ decay which can then be compared with the corresponding ft values in the $0+\rightarrow0+$ positron decays of Al^{26} and Cl^{34}. Using Gerhart's quoted end-point value of 1835 ± 8 kev and the calculations of Moszkowski and Jantzen,[28] one obtains an ft value of 3277 ± 63; with the end-point value of 1809.7 ± 7.8 kev reported here, one obtains an ft value of 3088 ± 56. These are to be compared with an ft of 3080 ± 80 for the Al^{26} decay assuming an end point of 3202 ± 10 kev from the work of Kington *et al.*[29] and of 3110 ± 120 for the Cl^{34} decay assuming an end point of 4500 ± 30 kev from the work of Kline and Zaffarano.[30] It is clear that the lower end-point value gives somewhat better agreement among the three ft values.

It should be noted that the reaction cycle $C^{12}(He^3,n)O^{14}-N^{14}(p,n)O^{14}-C^{12}(He^3,p)N^{14}\equiv0$ determines the Q value for the reaction $C^{12}(He^3,n)O^{14}$ and hence the threshold, in terms of the Q values for the (p,n) and (He^3,p) reactions listed. However neither of these is known with sufficient accuracy to be of use in checking the present result. No measurement of the

[27] Bockelman, Brown, Buechner, and Sperduto, Phys. Rev. **92**, 665 (1953).
[28] S. A. Moszkowski and K. M. Jantzen, University of California at Los Angeles Technical Report No. 10-26-55, 1956 (unpublished).
[29] Kington, Bair, Cohn, and Willard, Phys. Rev. **99**, 1393 (1955).
[30] R. M. Kline and D. J. Zaffarano, Phys. Rev. **96**, 1620 (1954),

(p,n) Q value exists other than that of Ajzenberg and Franzen[20] which has been adjusted by Mattauch *et al.*[14] to -5.934 ± 0.039 Mev, and no accurate measurement of the Q value of the (He^3,p) reaction has been made as yet.

Angular Distributions

At the outset of these experiments, it was realized that the low He^3 bombarding energy available would tend to complicate any analysis of the angular distribution measurements and that in particular any direct interaction or stripping contributions to the reactions might be obscured. From the experiments on deuteron stripping reactions there was hope, however, that even at low bombarding energy these contributions might dominate.

It is clear that the situation involved in the (He^3,p) and (He^3,n) reactions is considerably more complex than in the case of deuteron stripping or pickup reactions because of the necessity of capturing two nucleons with consequent complexity of the momentum balance in the problem. The (He^3,α) reaction should be directly comparable to the deuteron pickup reaction. The large cross section found for this reaction is strongly suggestive of direct interaction particularly when it is noted that in a compound nucleus picture these cross sections would require a probability for emission of an alpha particle of energy comparable to the barrier seven to nine times that for emission of a neutron and at least an order of magnitude greater than for emission of protons of comparable energy. Angular distributions of selected alpha-particle groups will be measured to look for evidence of Butler-type[31] stripping components as suggested by these measurements.

It should be noted that, from conservation of angular momentum and parity in the $C^{12}(He^3,p)N^{14}$ reaction, capture of a neutron-proton pair is forbidden, in the singlet case, to $1+$ states in N^{14} and is allowed for only s or d waves in the triplet case. Similarly, to $0+$ states in N^{14}, triplet capture is forbidden, as is singlet capture for all except s waves; to $0-$ states in N^{14}, only p-wave triplet capture is allowed.

It is possible to predict, in first approximation, the angular position of the maxima in the differential cross section for a stripping reaction by requiring conservation of linear momentum.[32] This means that the vectors representing the linear momenta of the incident, outgoing, and absorbed particles must triangulate. The first two momenta are obtained from the known energies and reaction kinematics; the third is obtained as $\mathbf{p}_c$, where $l\hbar=\mathbf{R}\times\mathbf{p}_c$. In this expression R is a characteristic radius in the problem, for convenience taken as the radius of the target plus that of the He^3 ion, and l is the usual stripping parameter equal to the number of units of orbital angular momentum carried by the absorbed particle.

As an example of the applicability of the model to (d,p) stripping reactions with comparable energies and targets, when applied to the $C^{13}(d,p)C^{14}$ and $C^{13}(d,n)N^{14}$ reactions at 4 Mev, the vector model predicts the peak intensities at laboratory angles of 0°, 24°, and 50° for $l=0$, 1, and 2, respectively. Detailed calculations using the same radii and energies in the Butler formulation of the stripping theory predict corresponding angles of 0°, 30°, and 60°. The experimentally observed $l=1$ peak is at 25°.[33] Similar agreement is found for $l=2$ transitions in the $F^{19}(d,p)F^{20}$ reaction, and in addition it is found experimentally that when the vectors do not triangulate the stripping patterns are much weaker or are smeared out beyond recognition.[26]

For orientation this model can be applied to the (He^3,p) reactions studied here to predict the angles at which peaks might be expected in the angular distributions if stripping plays an appreciable role. Figure 23 is

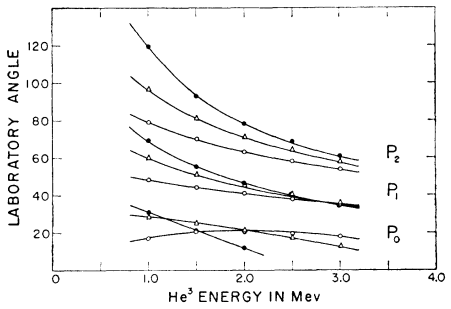

FIG. 23. Peak angles predicted from linear momentum conservation as a function of He^3 bombarding energy for the $C^{12}(He^3,p)N^{14}$ reaction. The open, triangular, and closed points identify the calculations for $l=1$, 2, and 3, respectively, where $l\hbar$ is the absorbed orbital momentum. In all cases, for $l=0$ the peak would of course be expected at 0°. Calculations for the proton groups to the ground and first two excited states of N^{14} are labeled P_0, P_1, and P_2, respectively.

a plot of these predicted peak angles for each of the three proton groups in the $C^{12}(He^3,p)N^{14}$ reaction where $l=1$, 2, and 3, as a function of the bombarding energy. This would predict that the curves shown in Figs. 10 and 12 to final states of identical character, $1+$, $T=0$, should have peaks at 0°, with perhaps a subsidiary peak between 50° and 80° (depending on energy) if an appreciable stripping contribution is present and, moreover, that the stripping contribution should be identical for both families of curves, neglecting Coulomb effects. Although a prominent peaking develops in the P_2 distributions at the higher energies, the two families are quite different and in general do not appear to satisfy the stripping requirements. Similarly, the curves shown in Fig. 11 to the $0+$, 2.3-Mev state would be expected to show prominent peaking at 0° if direct interaction contributions are large, whereas, of the three families of curves, these are least pronounced at 0°.

[31] S. T. Butler, Proc. Roy. Soc. (London) **A208**, 559 (1951).
[32] R. Huby, Proc. Roy. Soc. (London) **A215**, 385 (1952).
[33] D. A. Bromley, Phys. Rev. **88**, 565 (1952).

On the other hand, the distributions are not directly explicable as resulting from compound nucleus processes. The qualitative features of the distributions do not change rapidly with energy even though the yield curves show that several, and more probably a large number of levels in the compound nucleus are contributing to the reaction. The fact that the distributions are not symmetric about 90° could readily be attributed to interference contributions between the many levels available in the compound nucleus, and the difference between the distributions to the ground and second excited states in N^{14} may reflect the findings of Visscher and Ferrell[22] that, although these states have the same gross character, $1+$, $T=0$, the detailed components of the states' wave functions are quite different, in that the ground state is nearly pure $^3D_1$ and the 3.95-Mev state nearly pure $^3S_1$. However, since the emitted protons leading to the second excited state have lower energy by about 4 Mev than those to the ground state and would therefore be expected to be strongly influenced by both Coulomb and centrifugal barriers, it is somewhat surprising that the corresponding angular distributions should show appreciably more structure than those of the ground-state protons.

This situation is to be compared with that found in the measurements of the $Be^9(He^3,p)B^{11}$ angular distributions,[25] where again it is found that the qualitative features of the angular distributions do not change rapidly with energy. The distributions to the ground and second excited states of B^{11} are quite similar but markedly different from those to the first and third excited states, which in turn are quite similar. This apparent direct dependence on the characteristics of the final state, which is also found in the (d,p) stripping reaction to these states,[34] in that the first two show normal Butler stripping patterns whereas the second two do not, strongly suggests direct interaction contributions. These features of the distributions emphasize the desirability of having a detailed theoretical study of the (He^3,p) and (He^3,n) angular distributions. In the absence of any such theory, there is little that can be said about the significance of the Legendre polynomial expansion fits tabulated in Tables I and II. The fact that terms up to $P_6(\cos\theta)$ appear with appreciable intensity in at least some of the angular distributions is not inconsistent with a compound nucleus interpretation involving f-wave incident He^3 ions, since at a bombarding energy of 2.0 Mev, for example, the relative penetrability factors for s, p, d, f, and g waves on C^{12} are 1, 0.3, 0.05, 0.003, and 0.0001.[35] The angular distributions presented here for carbon do not conform to either the compound nucleus or the direct interaction pictures in detail, and it must be concluded that features of both are present.

ACKNOWLEDGMENTS

We are indebted to W. G. Cross, L. G. Elliott, W. T. Sharp, E. Vogt, H. E. Duckworth, and D. M. Van Patter for discussions regarding this work, to D. Huntley for performing many of the calculations, and to the operating staff for efficient running of the accelerator.

[34] S. A. Cox and R. M. Williamson, Phys. Rev. **99**, 631(A) (1955); and reference 11.

[35] Sharp, Gove, and Paul, Chalk River Report TPI-70, 1953 (unpublished).